



Fractal Riblets

Edoardo Alinovi,* Mattia Gribaudo,† and Alessandro Bottaro‡
University of Genova, 16145 Genova, Italy

DOI: 10.2514/1.J056985

Koch-like riblets that iteratively protrude toward the outside (the fluid region) or cave in at the wall are examined. The near-wall microscopic fluid problem is addressed by solving for the Stokes flow with a boundary element method, yielding slip lengths for all the surface shapes considered. Such lengths are then used in Navier boundary conditions of the macroscopic, turbulent problem, which is solved by direct numerical simulations. The results of the direct simulations demonstrate that inward-contracting riblets enjoy an additional drag reduction when compared to the base, triangular configuration, whereas outward-protruding riblets experience a skin-friction increase. The results are in excellent agreement with a theoretical model.

Nomenclature

b	=	riblet periodicity
b^+	=	riblet periodicity in wall units
C_f	=	friction coefficient
C_{f_0}	=	reference friction coefficient
D_α	=	fractal dimension
H	=	channel's half-height
$h_{ }$	=	longitudinal protrusion height
h_{\perp}	=	transverse protrusion height
U_b	=	bulk velocity
u	=	streamwise velocity component
u_τ	=	friction velocity
v	=	wall-normal velocity component
w	=	spanwise velocity component
x	=	streamwise coordinate
y	=	wall-normal coordinate
z	=	spanwise coordinate
α	=	angle at the base of the riblets
τ_w	=	wall shear stress
ΔC_f	=	difference between friction coefficients
Δh	=	difference between the protrusion heights
Δh^+	=	difference between the protrusion heights in wall units
Δx^+	=	streamwise grid spacing in wall units
Δy^+	=	wall-normal grid spacing in wall units
Δz^+	=	spanwise grid spacing in wall units
ν	=	fluid viscosity
ρ	=	fluid density

I. Introduction

RIBLETS are tiny grooves at the wall, aligned in the direction of the mean flow and regularly spaced along the transverse direction [1,2]. When properly designed, they are quite effective (under turbulent flow conditions) in reducing the skin friction below the value of a smooth surface by inhibiting the lateral movement of the near-wall coherent structures [3,4]. The main design parameter of riblets is their spanwise periodicity b ; because riblets, just like surface roughness, scale with boundary-layer inner variables, the dimensionless periodicity b^+ is typically used (i.e., b is normalized with the kinematic viscosity ν and the friction velocity $u_\tau = \sqrt{\tau_w/\rho}$, with τ_w as the statistically averaged wall shear stress and ρ as the density of the fluid). Skin-friction drag reduction by riblets is linear

with b^+ until $b^+ \approx 10$, and it is maximal when $b^+ \approx 15$. For b^+ above a value that can go from 20 to 35 (as function of their shape), riblets produce a drag increase because the near-wall vortices can settle within the grooves, increasing the shear stress [3,4]. In the linear regime (i.e., for sufficiently small b), the most effective way to understand the mechanism by which riblets operate has been proposed by Bechert et al. [5] and Luchini et al. [6,7], and it relies on decoupling the mathematical system into an inner problem and an outer problem. The equations describing the inner problem yield two protrusion heights (alternatively called slip lengths) that define two different virtual origins: one ($h_{||}$) for the longitudinal flow and one (h_{\perp}) for the crossflow. Protrusion heights are defined, for example, with respect to the tips of the riblets, which can be taken as the origin of the y axis, but this origin has no particular significance in relation to the flow. The significant parameter, independent of the choice of the origin, is $\Delta h = h_{||} - h_{\perp}$; it has been shown by Luchini [8] that the reduction in the skin-friction coefficient $\Delta C_f = C_f - C_{f_0}$ stems from a rigid displacement in y of the logarithmic law of an amount equal to Δh so that

$$\frac{\Delta C_f}{C_{f_0}} = -\frac{\Delta h^+}{(2C_{f_0})^{-1/2} + (2\kappa)^{-1}} \quad (1)$$

where C_{f_0} is the value of the coefficient for a smooth wall, κ is von Kármán's constant (which we can take equal to 0.41), and Δh^+ is the protrusion height difference scaled in inner variables. The aforementioned friction coefficient is defined as $C_f = 2\tau_w/\rho U_b^2$, with U_b as the bulk velocity.

Casting or rolling techniques have been employed in the past to manufacture plastic riblet sheets (see, for example, the patent by Marentic and Morris [9]); an interesting recent alternative consists of the embossing-curing method developed at Fraunhofer IFAM [10]. Other variants include multilayer processes patented by The Boeing Company to fabricate elastomeric [11] and shape-memory riblets [12], as well as a roller system to impress a microstructured pattern over a paint layer [13]. In all instances, the surface finish of the riblets is not the ideal, perfectly smooth one, and imperfections appear because of the rough material or the paint; furthermore, during usage, other contaminations may occur because of dirt or impact with insects. Thus, it becomes important to assess the effect of modifications in the riblet shape from the ideal design by considering the presence of micro- or nanoroughness elements upon the grooves.

Whether one considers random roughness or regular nanostructuring of the surface texture, it appears appropriate to start by examining the properties of fractal surfaces. The application of fractals to characterize rough surfaces dates back to the 1980s [14–17], upon the recognition that many rough surfaces demonstrate self-similar properties to some extent and over a certain range of scales. Today, etching techniques (plasma, laser, electrochemical), lithography (photo, x ray, etc.), deposition, and other approaches are routinely used to micro- and nanotexture surfaces for applications ranging from micro-electro-mechanical systems (MEMS) to magnetic storage devices.

Received 30 November 2017; revision received 28 February 2018; accepted for publication 3 March 2018; published online 25 April 2018. Copyright © 2018 by the American Institute of Aeronautics and Astronautics, Inc. All rights reserved. All requests for copying and permission to reprint should be submitted to CCC at www.copyright.com; employ the ISSN 0001-1452 (print) or 1533-385X (online) to initiate your request. See also AIAA Rights and Permissions www.aiaa.org/randp.

*Ph.D. Student, DICCA, Scuola Politecnica, via Montallegro 1.

†Graduate Student, DICCA, Scuola Politecnica, via Montallegro 1.

‡Professor, DICCA, Scuola Politecnica, via Montallegro 1.

II. Microscopic Problem

The microscopic near-wall configuration that we have considered consists of regular triangular grooves (see Fig. 1, left-side frames). The sides of the triangle are taken of equal length, and the angle at the base α is taken as equal to either 45, 60, 90 or 120 deg. The first fractal iteration, which is the second column in the figure, is achieved by dividing each side of the triangle into three segments and inserting an isosceles triangle (of the same vertex angle α) in place of the central segment so that each segment of the newly created fluid–solid boundary has equal length. The newly created rough boundary can either protrude toward the fluid (top row) or contract at the wall (bottom row). Figure 1 shows the first three iterations of the process, which yields what is known as the Koch curve for the case of $\alpha = 60$ deg. The angle α also defines the fractal dimension of each curve, characterizing its magnification. In fact, at each step of the iterative procedure, each line segment is replaced by $N = 4$ segments of equal length, with each self-similar copy which is

$$\frac{1}{S_\alpha} = \frac{1}{2(1 + \sin(\alpha/2))}$$

$$(u, v, w) = (y + h_\parallel, 0, y + h_\perp) \quad (2)$$

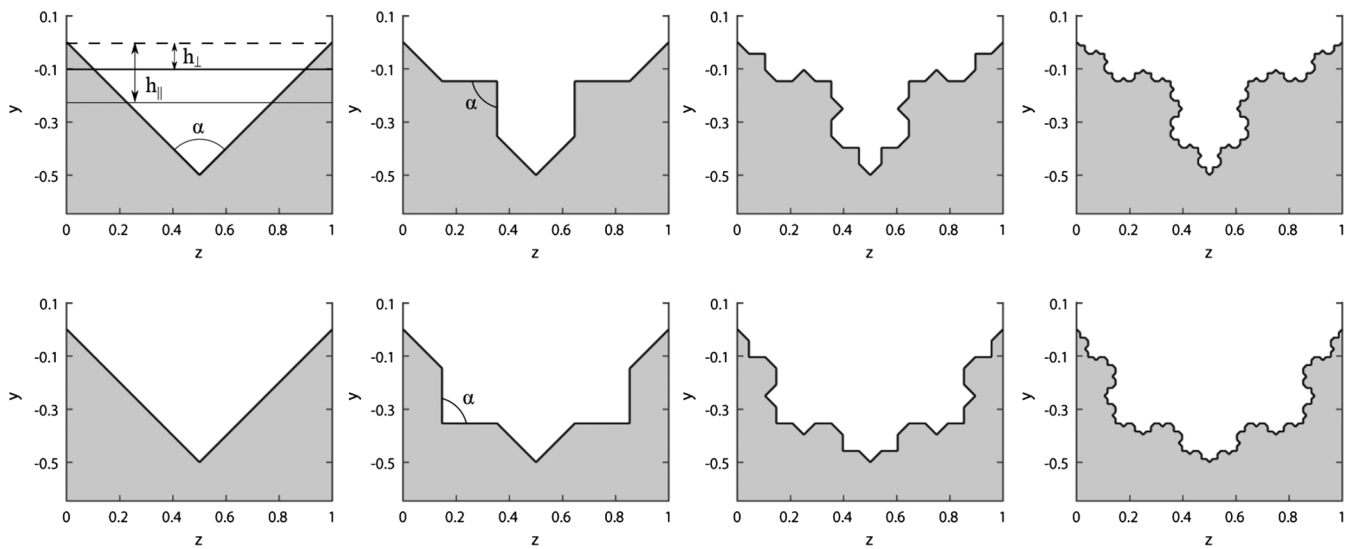


Fig. 1 Iterative process in the construction of fractal riblets for both outward- (top row) and inward-moving curves.

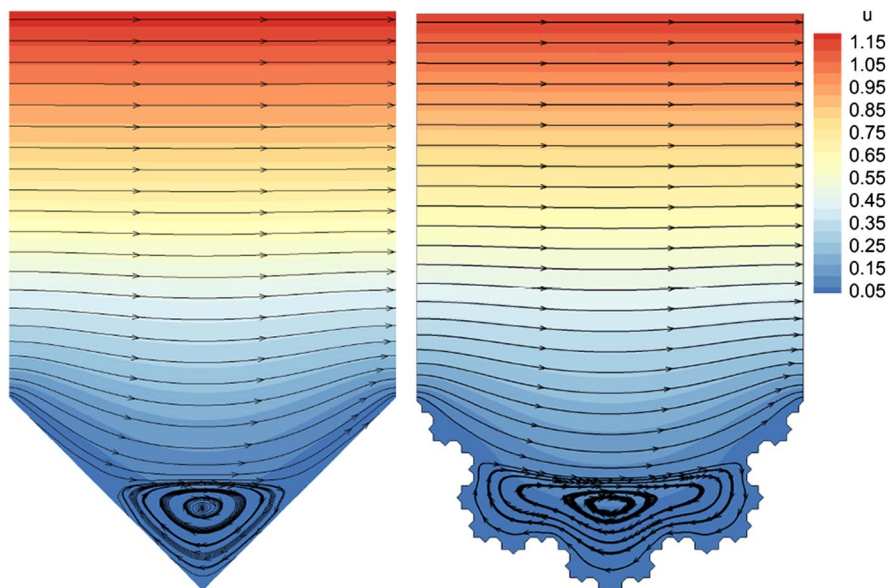


Fig. 2 Numerical solutions for the base configuration with $\alpha = 90$ deg (left frame) and for the third inward-moving iterate.

Table 1 Protrusions heights scaled by the spanwise periodicity b of the grooves

Angle α , deg		h_{\parallel}				h_{\perp}			
		it = 0	it = 1	it = 2	it = 3	it = 0	it = 1	it = 2	it = 3
45	<i>i</i>	0.1842	0.1851	0.1872	0.1885	0.0815	0.0816	0.0818	0.0819
60	<i>i</i>	0.1706	0.1733	0.1762	0.1775	0.0803	0.0806	0.0807	0.0808
90	<i>i</i>	0.1396	0.1464	0.1495	0.1506	0.0778	0.0779	0.0782	0.0783
	<i>o</i>	0.1396	0.1117	0.0989	0.0949	0.0788	0.0744	0.068	0.0659
120	<i>i</i>	0.1026	0.1112	0.1138	0.1146	0.0704	0.0715	0.0723	0.0725
	<i>o</i>	0.1026	0.0819	0.0755	0.0737	0.0704	0.0604	0.0554	0.0541

with u , v , and w , respectively, as the streamwise, wall-normal, and spanwise velocity components; these are scaled with the inner velocity scale, i.e.,

$$b \frac{\partial u}{\partial y} \Big|_{y \rightarrow \infty}$$

and lengths are normalized with the microscopic length scale b . The two protrusion heights are drawn (qualitatively) in the top, left frame of Fig. 1 and are measured with reference to the (arbitrary) origin of the y axis.

The numerical solution of the microscopic equations is carried out in a domain of spanwise dimension equal to one and a vertical dimension sufficiently large for the asymptotic solution to be established (the upper boundary can safely be taken at $y_{\infty} = 4$). It is accomplished by a boundary element method [19,20], which is extensively validated against results in the literature. The calculation of the slip lengths takes advantage of the asymptotic relations [Eq. (2)] for the velocity components, which are directly measured by our numerical code at $y = y_{\infty}$. The dimensionless protrusion heights are then simply

$$(h_{\parallel}, h_{\perp}) = (u(y_{\infty}) - y_{\infty}, w(y_{\infty}) - y_{\infty})$$

Examples of the numerical results are given in Fig. 2. The isocolors in the figure define the streamwise velocity (which arises from the solution of a Laplace equation for u [3]), whereas the streamlines (with arrows) represent the secondary velocity vector (v , w) stemming from the solution of a two-dimensional Stokes problem in the (y, z) plane [6]. A larger secondary vortex appears in the image in the right frame, which is a feature associated to larger values of both protrusion heights.

The results in terms of protrusion heights for both inward-moving (“*i*”) and outward-moving (“*o*”) surfaces are reported in Table 1 for the base configuration (indicated by “it = 0”) and up to the third iteration. The outward protruding results for the cases of $\alpha = 45$ deg and $\alpha = 60$ deg are not present in the table (nor in Fig. 3) because the vertices of the triangles added in the first iteration touch one another, creating two disconnected fluid regions.

The distances h_{\parallel} and h_{\perp} define virtual walls for, respectively, the longitudinal and transverse velocity profiles. The significant length scale, independent of the choice of the origin, is (however) Δh , which

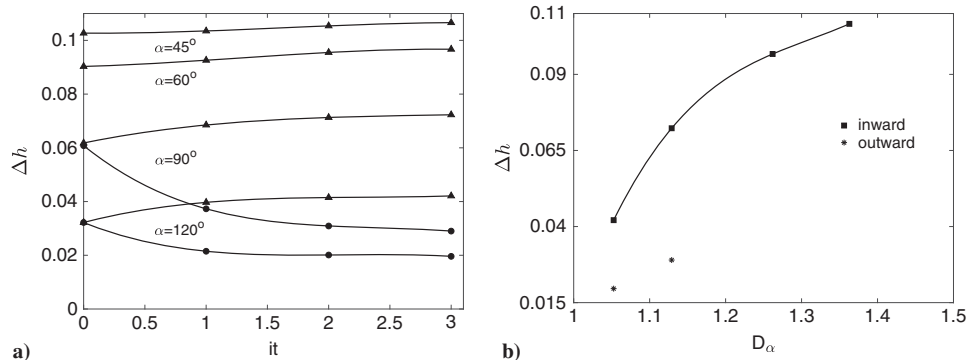
is displayed in Fig. 3; Fig. 3a shows that Δh increases as the wall moves inward (triangular symbols) for all α . By the third iteration, the results are essentially converged and further iterations on the fractal curve produce negligible modifications of Δh for both the *i* and the *o* cases. The variation in Δh between the initial configuration (it = 0) and the last iteration (it = 3) quantifies, for each opening angle α , the additional drag reduction which we might expect when using fractal riblets [as in Eq. (1)]. Such a variation is equal to 4% when $\alpha = 45$ deg, 7% when $\alpha = 60$ deg, 17% when $\alpha = 90$ deg, and almost 31% when $\alpha = 120$ deg. Thus, the least efficient riblets tested (the triangular ones, with vertex angles of $\alpha = 120$ deg) are those that have the most to gain by hierarchical micro- and nanostructuring. When α is equal to 45 deg, we have the best results among all cases considered (in terms of drag reduction), but we might expect even better results by further reducing α or, equivalently, increasing D_{α} , as Fig. 3b suggests (the values of Δh reported refer to it = 3). The close correlation between Δh and ΔC_f will be examined in the next section. It is important to stress, however, that the best results found here are not the absolute best results that could be found; it is possible, for example, that (hierarchically) nanostructured blade riblets yield even larger values of Δh . The search for the optimal riblet shape is left for future work.

III. Macroscopic Problem

The pressure-driven turbulent flow in a channel is now considered, and Navier boundary conditions are applied over smooth, fictitious walls. The channel considered is shown in Fig. 4; it is $2\pi H$ long along x and πH along the span z , with H as the half-distance between the two walls. The boundary conditions are periodic along x and z , whereas the Navier slip conditions are imposed on the upper and lower surfaces, which are imagined to be micro-/nanostructured in the same manner. If $y = 0$ is the position of the lower wall, and H is the macroscale employed to normalize distances, the dimensionless conditions at $y = 0$ and 2 read as follows:

$$u(x, 1 \pm 1, z) = \mp h_{\parallel} \frac{b}{H} \frac{\partial u}{\partial y} \Big|_{y=1 \pm 1} \quad (3)$$

$$v(x, 1 \pm 1, 0) = 0 \quad (4)$$


Fig. 3 Protrusion height difference for all the cases considered as a function of the a) fractal iteration and b) fractal dimension.

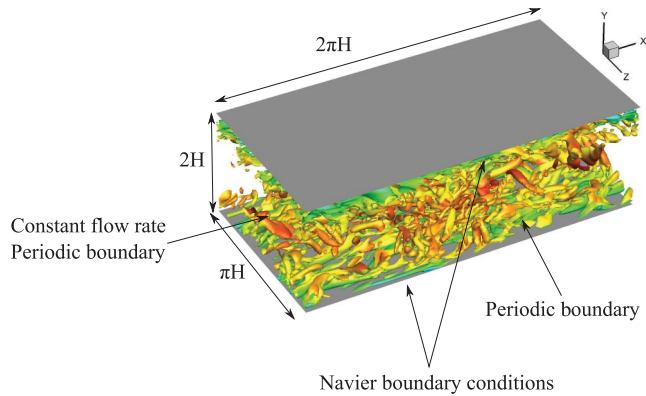
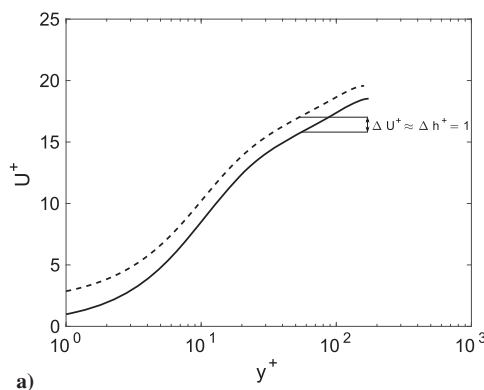


Fig. 4 Image of the configuration studied, with dimensions and boundary conditions. The colored images drawn within the two gray surfaces represent the coherent flow structures visualized via the Q criterion.

$$w(x, 1 \pm 1, z) = \mp h_{\perp} \frac{b}{H} \frac{\partial w}{\partial y} \Big|_{y=1 \pm 1} \quad (5)$$

We stress the fact that the positions of $y = 0$ and $y = 2$, where these boundary conditions are applied, are arbitrary and the Navier slip condition is but a first-order approximation of the true boundary condition to be enforced at the fictitious upper and lower walls. As such, an error, which depends on the aspect ratio of the surface irregularities [21], is committed when using Eqs. (3–5). Furthermore, as already stated earlier, the results are only valid in the linear limit of the riblets, i.e., when the periodicity of riblets scaled in wall units b^+ is around 10 at most.

The flow rate through the channel is maintained constant via a streamwise forcing term in the Navier–Stokes equations; the Reynolds number for all cases treated is $Re = U_b H / \nu \approx 2800$, which translates to $Re_{\tau} = u_{\tau} H / \nu \approx 180$. These conditions correspond exactly to those employed by Kim et al. [22] in their study of turbulence in a plane channel, as well as by Min and Kim [23] in their later work on the effect of superhydrophobic surfaces upon turbulence. The numerical technique used here is similar to that by Min and Kim and is based on a finite volume semi-implicit fractional step method that is second-order accurate in both space and time, which has been amply validated [24]. Our resolution is better than that employed by Min and Kim: our first grid point is at $y^+ = 0.025$ (against their value of 0.3), and the grid is stretched along y by the use of a hyperbolic tangent distribution; the uniform values of Δx^+ and Δz^+ in our case are, respectively, 7 and 4.4, which are smaller than the values used by Min and Kim (equal, respectively, to 10 and 5). The accuracy of the grid used here guarantees, in particular, accurate predictions of the velocity gradients at the wall. Like in the case of Min and Kim, examination of the spectra at different wall-normal positions reveals the expected decay and is reassuring in terms of the resolution employed.



An example of numerical solutions, for both no-slip and slip walls, is displayed in Fig. 5. The ribleted case focused upon is that for which $\Delta h^+ = 1$. Whereas the statistics (Fig. 5b) show only a small difference between the two configurations, the mean streamwise velocity (Fig. 5a) displays the expected trend, with the logarithmic region of the flow shifted upward by the presence of the riblets, at each given y^+ by a quantity equal to $\Delta U^+ \approx \Delta h^+$. Corresponding shifts occur when different protrusion heights are simulated (not shown).

The computed smooth-wall skin-friction coefficient is equal to $C_{f_0} = 0.0081$, which is very close to the value of Kim et al. [22]. As far as the values of Δh^+ are concerned [because, from Fig. 3, we observe that Δh is at the most around 0.1 (in units of b)], it is $\Delta h^+ < 0.1b^+$. Given that the linear regime of riblets exists until b^+ is on the order of 10, we must limit the study to Δh^+ up to about one. This sets the limits of validity of the current study. The computed ratios $|\Delta C_f|/C_{f_0}$ are plotted in Fig. 6 for all the cases considered, together with the correlation given by Eq. (1) and the results by Min and Kim [23]. The results demonstrate a drag reduction in excess of 10% when Δh^+ reaches one; the agreement of the results with both the previous numerical solutions and the analytical expression by Luchini [8] is very good, confirming both the linear dependence of the skin-friction drag reduction with Δh and the interest, when skin-friction reduction is aimed at, in using the inward fractal configuration (which yields larger values of Δh^+) rather than the

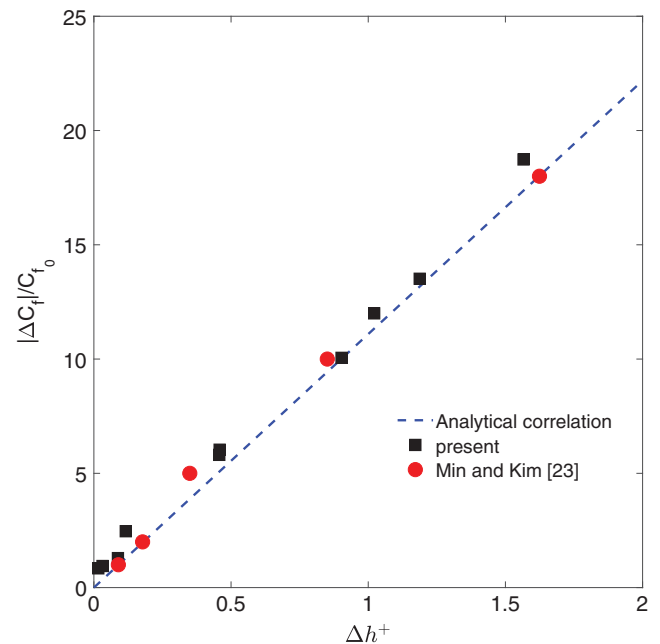


Fig. 6 Linear correlation between the percentage drag reduction and the protrusion height difference.

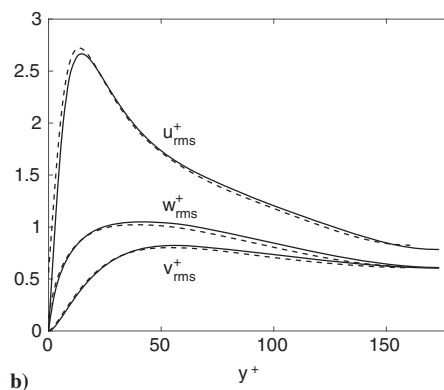


Fig. 5 Comparison between the a) mean velocity profiles and b) turbulent statistics between the standard no-slip walls (solid lines) and ribleted walls for $\Delta h^+ = 1$ (dashed lines).

outward one. Among the possible fractal configurations, it is advisable (on the basis of the results reported here) to employ those with the largest fractal dimension D_α .

IV. Conclusions

Fractal riblets have been studied as a first step to model either the presence of random roughness or the hierarchical micro- and nanostructuring of a basic triangular groove shape. The key result here is the solution found in terms of a protrusion height difference: a parameter that describes the relative virtual origin of the longitudinal near-wall motion when compared to the crossflow one. The results demonstrate that the presence of micro- and nanoindentations can either improve things, in terms of skin-friction drag reduction, or deteriorate them, depending, respectively, on whether the basic shape is successively indented toward the inside or protrudes toward the outside. In the inward case, when larger viscous secondary vortices can be accommodated within the grooves, the larger values of Δh (and thus the skin-friction reduction ΔC_f) correlate well with the fractal dimension of the surface, thus suggesting a possible way to structure walls in order to reduce drag.

Acknowledgments

We acknowledge Paolo Luchini for several interesting discussions on the subject of riblets and Alfredo Pinelli for both interactions on the issue of direct numerical simulations and for providing the computational code employed in the macroscopic simulations. Preliminary calculations to validate the boundary element code have been carried out by Giovanni Trovato.

References

- [1] Walsh, M. J., "Riblets as a Viscous Drag Reduction Technique," *AIAA Journal*, Vol. 21, No. 4, 1983, pp. 485–486. doi:10.2514/3.60126
- [2] Walsh, M. J., "Viscous Drag Reduction in Boundary Layers," *Progress in Astronautics and Aeronautics*, Vol. 123, edited by D. M. Bushnell, and J. N. Hefner, AIAA, Washington, D.C., 1990, pp. 203–261. doi:10.2514/5.9781600865978.0203.0261
- [3] Bechert, D. W., and Bartenwerfer, M., "The Viscous Flow on Surfaces with Longitudinal Ribs," *Journal of Fluid Mechanics*, Vol. 206, Sept. 1989, pp. 105–129. doi:10.1017/S0022112089002247
- [4] Choi, H., Moin, P., and Kim, J., "Direct Numerical Simulation of Turbulent Flow over Riblets," *Journal of Fluid Mechanics*, Vol. 255, Oct. 1993, pp. 503–539. doi:10.1017/S0022112093002575
- [5] Bechert, D. W., Bartenwerfer, M., and Hoppe, G., "Turbulent Drag Reduction by Nonplanar Surfaces—A Survey on the Research at TU/DLR Berlin," *Structure of Turbulence and Drag Reduction*, edited by A. Gyr, Springer, Berlin, 1990, pp. 525–543.
- [6] Luchini, P., Manzo, F., and Pozzi, A., "Resistance of a Grooved Surface to Parallel Flow and Cross-Flow," *Journal of Fluid Mechanics*, Vol. 228, July 1991, pp. 87–109. doi:10.1017/S0022112091002641
- [7] Luchini, P., Manzo, F., and Pozzi, A., "Viscous Eddies over a Grooved Surface Computed by a Gaussian-Integration Galerkin Boundary-Element Method," *AIAA Journal*, Vol. 30, No. 8, 1992, pp. 2168–2170. doi:10.2514/3.11200
- [8] Luchini, P., "Reducing the Turbulent Skin Friction," *European Congress on Computational Methods in Applied Sciences and Engineering—Proceedings of 3rd ECCOMAS CFD Conference*, edited by J. A. Désidéri, Wiley, Chichester, England, U.K., 1996, pp. 466–470.
- [9] Marentic, F. J., and Morris, T. L., 3M Company, St Paul, MN, U.S. Patent Application for "Drag Reduction Article," Application No. US06740239, May 1985, <https://patents.google.com/patent/US5069403A/en> [retrieved 2018].
- [10] Kordy, H., "Process Abilities of the Riblet-Coating Process with Dual-Cure Lacquers," *CIRP Journal of Manufacturing Science and Technology*, Vol. 11, No. 8, 2015, pp. 1–9. doi:10.1016/j.cirpj.2015.08.003
- [11] Rawlings, D., and Burg, A., U.S. Patent Application for "Elastomeric Riblets," Application No. 12566927, 2010, <http://www.google.la/patents/US20100282909> [retrieved 2018].
- [12] Rawlings, D., and Schneider, T., U.S. Patent Application for "Shape Memory Riblets," Application No. 12361882, 2010, <https://www.google.com/patents/US20100187360> [retrieved 2018].
- [13] Travis, M. H., European Patent Application for Drag Reduction Riblets Integrated in a Paint Layer," Application No. EP20150177084, 2016, <https://www.google.com/patents/EP2982599A1?cl=en> [retrieved 2018].
- [14] Mandelbrot, B. B., Passoja, D. E., and Paullay, A. J., "Fractal Character of Fracture Surfaces of Metals," *Nature*, Vol. 308, No. 5961, 1984, pp. 721–722. doi:10.1038/308721a0
- [15] Gagnepain, J. J., and Roques-Carmes, C., "Fractal Approach to Two-Dimensional and Three-Dimensional Surface Roughness," *Wear*, Vol. 109, No. 1, 1986, pp. 119–126. doi:10.1016/0043-1648(86)90257-7
- [16] Frederick, F. L., "Scaling Law for Contoured Length of Engineering Surfaces," *Journal of Applied Physics*, Vol. 62, No. 6, 1987, pp. 2570–2572. doi:10.1063/1.339427
- [17] Majumdar, A., and Bhushan, B., "Role of Fractal Geometry in Roughness Characterization and Contact Mechanics of Surfaces," *Journal of Tribology*, Vol. 112, No. 2, 1990, pp. 205–216. doi:10.1115/1.2920243
- [18] Crowdy, D., "Slip Length for Longitudinal Shear Flow over a Dilute Periodic Mattress of Protruding Bubbles," *Physics of Fluids*, Vol. 22, No. 12, 2010, Paper 121703. doi:10.1063/1.3531683
- [19] Alinovi, E., and Bottaro, A., "A Boundary Element Method for Stokes Flows with Interfaces," *Journal of Computational Physics*, Vol. 356, March 2018, pp. 261–281. doi:10.1016/j.jcp.2017.12.004
- [20] Alinovi, E., and Bottaro, A., "Apparent Slip and Drag Reduction for the Flow over Superhydrophobic and Lubricant-Impregnated Surfaces," *Physical Review Fluids* (submitted for publication).
- [21] Luchini, P., "Linearized No-Slip Boundary Conditions at a Rough Surface," *Journal of Fluid Mechanics*, Vol. 737, Dec. 2013, pp. 349–367. doi:10.1017/jfm.2013.574
- [22] Kim, J., Moin, P., and Moser, R., "Turbulence Statistics in Fully Developed Channel Flow at Low Reynolds Number," *Journal of Fluid Mechanics*, Vol. 177, April 1987, pp. 133–166. doi:10.1017/S0022112087000892
- [23] Min, T., and Kim, J., "Effects of Hydrophobic Surface on Skin-Friction Drag," *Physics of Fluids*, Vol. 16, No. 7, 2004, pp. L55–L58. doi:10.1063/1.1755723
- [24] Pinelli, A., Naqavi, I. Z., Piomelli, U., and Favier, J., "Immersed-Boundary Methods for General Finite-Difference and Finite-Volume Navier–Stokes Solvers," *Journal of Computational Physics*, Vol. 229, No. 24, 2010, pp. 9073–9091. doi:10.1016/j.jcp.2010.08.021

P. Givi
Associate Editor